ISSN 2176-5480

22nd International Congress of Mechanical Engineering (COBEM 2013)
November 3-7, 2013, Ribeirão Preto, SP, Brazil

COMPARATIVE STUDY OF VORTICITY FIELDS GENERATED BY CYLINDRICAL BODIES UNDERGOING FORCED ROLLING MOTION

Martins, F.P.R.
Escola Politécnica da Universidade de São Paulo
Av. Prof. Mello Moraes 2231, Cidade Universitária, São Paulo, São Paulo
flavius.martins@usp.br

Trigo, F.C.
Escola Politécnica da Universidade de São Paulo
Av. Prof. Mello Moraes 2231, Cidade Universitária, São Paulo, São Paulo
trigo.flavio@usp.br

Fleury, A.T.
Centro Universitário da Fundação de Ensino Inaciano
Av. Humberto de Alencar Castelo Branco, 3972, São Bernardo do Campo, São Paulo
agfleury@fei.edu.br

Ponge-Ferreira, W.J.A.
Escola Politécnica da Universidade de São Paulo
Av. Prof. Mello Moraes 2231, Cidade Universitária, São Paulo, São Paulo
ponge@usp.br

Abstract. *The focus of the present paper is the application of image processing methods to extract quantitative information from velocity fields generated by cylindrical bodies undergoing forced harmonic rolling motion around a fixed axis positioned transversally to a tank facility at the still free surface level. Different geometries were considered, including chine and round bilges, with and without bilge keels. The surrounding velocity field was evaluated through the Particles Image Velocimetry (PIV) technique at discrete phases of sequential cycles of the movement and a method based on the analysis of the velocity tensor was adopted to identify the vortices diffused by the flow. Finally, the application of classical image segmentation techniques permitted to estimate statistics of the vorticity field which may be furtherly used to compare the hydrodynamics performance of the oscillating bodies.*

Keywords: *vortex identification; decomposition of motion; PIV; image processing.*

1. INTRODUCTION

Thanks to the development of numerous robust commercial and academic PIV systems, obtaining high resolution maps of velocity fields has increasingly becoming a low-cost task easily performed by the hydrodynamics laboratories staff. As a consequence, very large databases of PIV images have been added to the set of measurements issued by experiments carried out on towing tanks, demanding to the experts an extra effort to be properly analysed and interpreted. Also, PIV velocity maps are typically contaminated with randomly spurious vectors, mainly due to inadequate seeding and to the presence of reflective surfaces. The hugeness of the data and the necessity of performing systematic noise removal requires the adoption of automatic PIV image postprocessing methods. Furthermore, to completely automate the analysis task, it is necessary to build computer vision algorithms based on measurement metrics capable to emulate the expert visual ability to properly interpret velocity fields, which is a hurdle difficult to surmount. Such goals have being focused by numerous articles recently reported in the literature.

Noise removal and missing data problems can be achieved by several different methods. Nogueira et al. (1997), for instance, elliminate the spurious vectors on PIV images severelly affected by improper seeding by a three-steps sequence encompassing localization of the coherent zones, tracking off the high gradients of the field and finally filter interpolation of the previously processed map. Baur and Koengeter (2000), analysing the flow around a fixed obstacle mounted on a channel, applied a time-averaging based technique to smooth the PIV images. After testing classical low-pass filters to elliminate spurious velocity vectors from PIV image data, Yang et al. (2011) concluded that a proper sized median filter could significantly improve the accuracy of the measurements.

Having the measurement noise being properly filtered out from the data, quantitative information of the flow can be obtained through a palette of techniques aimed at decomposing the velocity field into simpler components and using those components to construct metrics for the observed phenomena. Rao and Jain (1992) proposed a domain independent method to both qualitatively and quantitatively describe 2D flow fields by associating proper symbolic representation to specific texture patterns. Adrian et al. (2000) presented the main ideas concerning methods for analysing the original flow field, encompassing Reynolds, vorticity, Galilean and low-pass filtering decomposition.

ISSN 2176-5480

Jiang et al. (2004) presented a comparative study of nine classes of algorithms for detecting vortex patterns on flow fields. Finn et al. (2005) implemented a parallel algorithm (validated against synthetically generated flow fields exhibiting vortex knots evolving according to the Navier-Stokes equations) which identify vortices by looking for local maxima of the line integral of vorticity around closed paths. After presenting a rigorous comparative study of three techniques for identifying vortices, based on local analysis of the velocity gradient tensor, Chakraborty et al. (2005) proposed a new more robust method that include to those criteria a measure of spiralling compactness of the vortices orbits. Advocating that flow field double decomposition techniques, as the majority ones based on the local velocity gradient tensor, can not be appropriate for dealing with many types of fluid mechanics problems, Kolár (2007) proposed a triple decomposition technique, able to separate the shear and the swirling components of the vorticity field.

In the present article we discuss the results concerning the analysis and interpretation of a large set of PIV time images sequences of flow fields generated by four distinct cylindrical bodies undergoing harmonic rolling motion. The procedure adopted for analysing the images followed the steps usually found in the literature: noise removal, flow field decomposition and statistical analysis based on metrics derived from the field components.

2. EXPERIMENTAL SET UP

The experiments were conducted on a channel (Fig. 1) circa 25 meters long, 1.0 meter wide and 0.8 meters deep, having on one of its side walls a 2 meters long transparent window through which the flow can be properly visualized.

Figure 1. Channel used in the tests.

A cylindrical body was positioned transversally to the tank and forced to harmonically roll around a fixed axis situated near the free surface level. During the experiments, four distinct cylindrical bodies were adopted (Fig. 2): 1) round bilge with no bilge keel; 2) hard chine with no bilge keel; 3) round bilge with a small bilge keel; 4) round bilge with a large bilge keel.

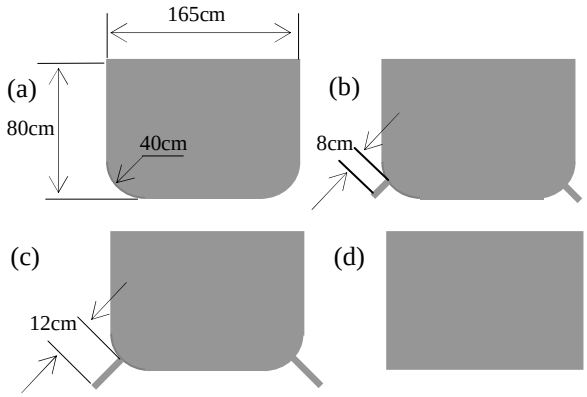

Figure 2. Models used in the tests: (a) round bilge, no bilge keel; (b) round bilge, small bilge keel; (c) round bilge, large bilge keel; (d) hard chine, no bilge keel

ISSN 2176-5480

Although a total of 140 tests were applied to the cylindrical bodies, in this article we will focus a group of only four tests performed on the same basis using each of the four models referred above. In these tests, a controlled forced torque was applied to the rotation axis in order to impose to the cylindrical body a simple harmonic motion of 8° amplitude and 2Hz frequency.

Using Lavision^{TM} PIV system, a sequence of 100 flow images, corresponding to the long term velocity fields due to the oscillating bodies were generated at a rate of 4 frames/sec, following the grabbing cycle indicated in Fig. 3.

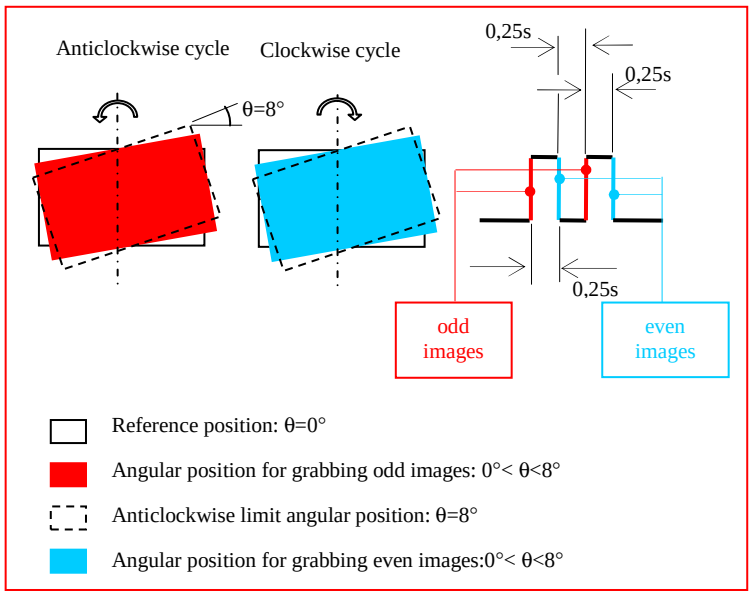

Figure 3. Image grabbing cycle of the oscilating rolling motion

In the next two sections we present the methodology used to postprocess those images.

3. IMAGE NOISE REMOVAL

As it can be seen in Fig. 3, the generated PIV images are intensely affected by noise caused both by improper seeding and by the presence of reflective artifacts in the scene.

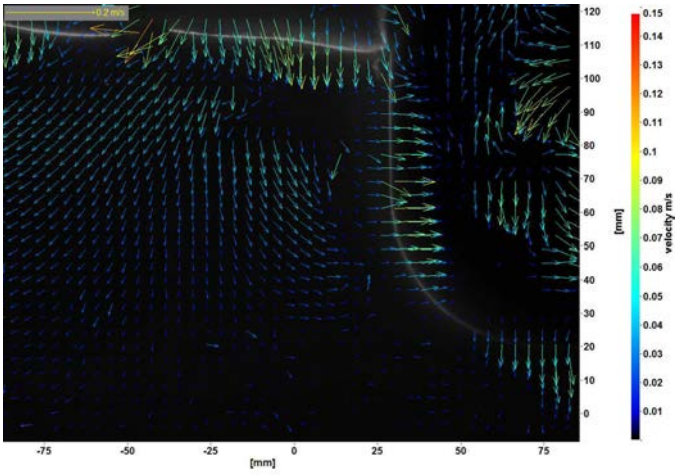

Figure 3. Flow field images generated by the PIV system

To remove the spurious vector velocities found in the region covered by the hull and near the free water surface, we applied a morphology-based image processing algorithm written in Matlab^{TM}, that, starting from PIV crude images like the image **I** shown at Fig. 5a, generates a validating mask of the field (Fig.5h) through the steps presented below:

1. I_1=globalThresholding(I) (Fig 5b);
2. I_2=localThresholding(I,10,100) (Fig 5c);

ISSN 2176-5480

3. $I_3=I_2 \oplus SE(circle,1) \mid I_1$ (Fig 5d);
4. $I_4=labelled(I_3)$;
5. I_5=image containing the only object of I_4 that has the nearest point to the bottom right frame corner (Fig. 5e);
6. $I_6= I_5$+poligon limited by the frame borders and the contour line in I_5; (Fig. 5f);
7. $I_7=I_6 \oplus SE(circle,4)$ (Fig.5g);
8. $I_8=(Not(I_7)-BorderObjects(Not(I_7))) \oplus (circle,4)$ (Fig. 5h);

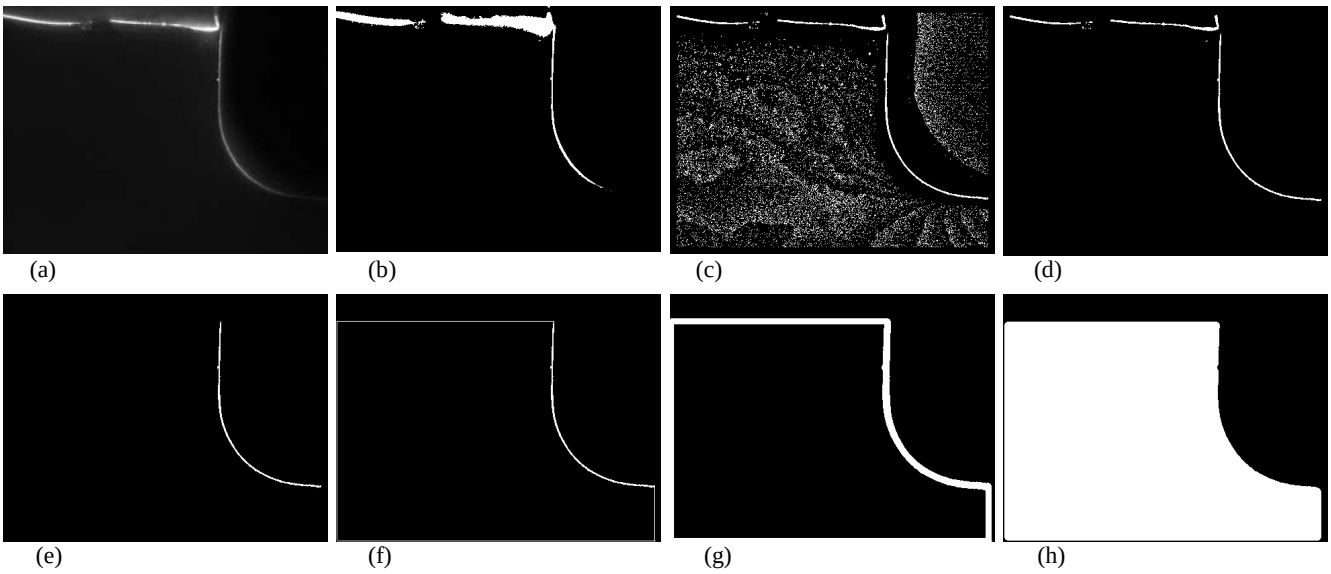

Figure 5. Morphological procedure to generate an image flow field validating mask

In the preceding algorithm, global thresholded image I_1 is obtained through Otsu´s method (Otsu's, 1979) while local thresholding image I_2 is the the result of applying to image I the Niblack's algorithm (Niblack, 1986), adopting 10×10 neighborhoods and 100% weight for the image local standard deviation values. Image I_3 results from a conditional dilation of the image I_1 (Serra, 1982) using image I_2 as the reference image and a circle of radius 1 as the structuring element. Construction of image I_6 requires finding the connected object which has the right-most and bottom-most pixel and connecting this object to the image frame using proper horizontal and vertical lines. Image I_7 results from a dilation of image I_6, using a circle of radius 4 as the structuring element. Finally, to obtain the validating mask image I_8, it is necessary to elliminate the border objects (Haralick and Shapiro, 1991) of the negative of image I_7, and dilating the resultant image using a structuring element circle of radius 4.

Concerning the removal of the outlier vectors due to improper seeding from the velocity field, it is sufficient to apply a median filter of size 3×3 both to the $V_x=V_x(x,y)$ and $V_y=V_y(x,y)$, where (x,y) are points for which $I_8(x,y)=1$.

4. FLOW FIELD DECOMPOSITION

Although the decomposition of the motion could be achieved by different means, the characteristics of the investigated flow and of the measurements provided by the tests lead us to follow a Galilean invariant approach to separate the turbulent eddies diffused in the flow from its velocity convection components.

Amongst the numerous identification vortex algorithms described in the literature, we adopted the one proposed by Chakraborty et al. (2005), whose robustness has been proven to be superior than their counterparts based on the analysis of critical points of the local velocity gradient tensor. In order to undertake its pattern matching task, the referred algorithm assumes that 'when observed on a frame moving with its core, a vortex is a fluid structure that exhibits swirling (so, no shearing) local flow and presents a compact orbit'.

The above definition can be quantitatively translated into two Galilean invariant metrics based on the local velocity gradient tensor: 1) swirling strength; 2) vortex compactness.

For 2-D flows, the local gradient velocity tensor, $\nabla\vec{v}$, is given by:

$$\nabla\vec{v} = \begin{bmatrix} \partial v_x/\partial x & \partial v_x/\partial y \\ \partial v_y/\partial x & \partial v_x/\partial y \end{bmatrix} \quad (1)$$

Therefore, $\nabla\vec{v}$ either has two real eigenvalues or a pair of complex conjugate ones, in the form

ISSN 2176-5480

$$\lambda = \lambda_{Cr} \pm i \cdot \lambda_{Ci} \tag{2}$$

If the above condition is satisfied, the vortex has a local pure swirling motion and its period for one revolution is given by:

$$T = 2\pi / |\lambda_{Ci}| \tag{3}$$

Furthermore, considering two points in the vortex core that are initially separated by the distance r_0, it can be shown (Chakraborty et al., 2005) that, after n revolutions those points will be separated by a distance r_f given by

$$r_f = r_0 \cdot e^{2\pi n \left| \frac{\lambda_{Cr}}{\lambda_{Ci}} \right|} \tag{4}$$

Consequently, for small values of $\lambda_{Cr} / \lambda_{Ci}$ the flow exhibits a compact and clear spiralling path while higher values of this parameter indicates a rapid material radial spreading, a behavior that is atypical for real vortices.

Using the criteria succintly mentioned above, we applied the following algorithm to identify vortices in the four sets of temporal sequences of PIV noise-filtered images:

for all valid values of (x,y) {
calculate $\nabla \vec{v}(x, y)$;
calculate the eigenvalues of $\nabla \vec{v}(x, y)$;
if $|\lambda_{Ci}| > 0.6$ and $|\lambda_{Cr} / \lambda_{Ci}| < 0.2$
then (x,y) ∈ vortex };

Figs. 6a-d show the vorticity distribution imagens $\mathbf{I_v}$, issued by the above algorithm applied to instantaneous flow images concerning the four types of cylindrical bodies tested in the experiments. The vortical areas correspond to the bright regions of the images.

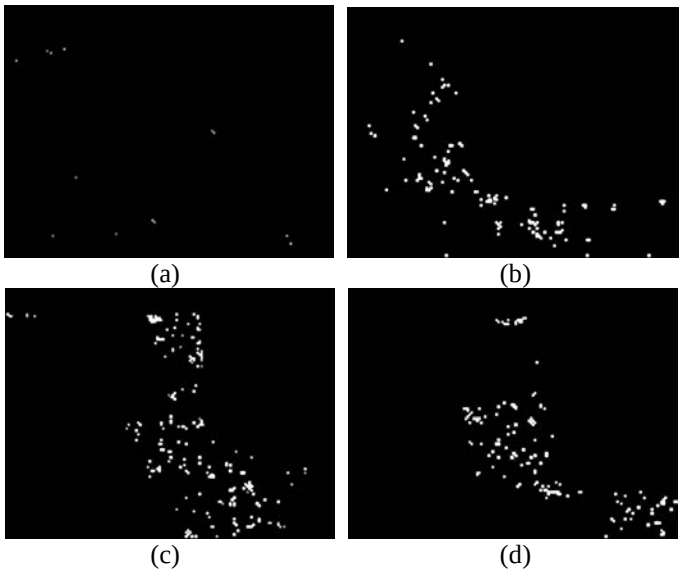

Figure 6. Instantaneous vortex distribution in flows generated by: (a) round bilge without bilge keel; (b) round bilge with small bilge keel; (c) round bilge with large bilge keel; (d) hard chine without bilge keel

5. QUANTITATIVE EVALUATION OF THE VORTICITY FIELDS

The four sets of vorticity distribution images sequences $\mathbf{I_v}(t)$ were submitted to a straightforward image segmentation process consisting of a chain of thresholding and connect components labelling (Horn, 1986) algorithms that transform $\mathbf{I_v}(t)$ in a set of n separated regions, each one associated to an individual vortex. This way, average properties of the vorticity fields can be easily estimated after calculating individual properties of the vortical areas.

Despite numerous geometrical, kinematics and dynamical properties can be associated to those segmented regions of the vorticity field, we verified that the temporal evolution of only three average vortex properties provide the means to compare the hydrodynamic performance of the cylindrical bodies concerning rolling motion. The referred properties

ISSN 2176-5480

are the following: vortex average equivalent diameter, vortex average velocity and vortex average Reynolds number, given, respectively by

$$\overline{D} = \frac{1}{n}\sum_{i=1}^{n} d_i = \frac{1}{n}\sum_{i=1}^{n} 2\sqrt{A_i/\pi} \tag{5}$$

$$\overline{V} = \frac{1}{n}\sum_{i=1}^{n} v_i = \frac{1}{n}\sum_{i=1}^{n} \Omega_i \pi d_i \tag{6}$$

$$\overline{\mathrm{Re}} = \frac{1}{n}\sum_{i=1}^{n} \mathrm{Re}_i = \frac{1}{n}\sum_{i=1}^{n} \frac{v_i d_i}{\nu} \tag{7}$$

where A_i and $\Omega_i = 2\pi/T_i$ are, respectively, the area and the angular velocity associated to the ith connected object of thresholded image $I_v(t)$; ν is the kinematic viscosity of the water.

Figures 6 to 9 represent the temporal evolution of the three above mentioned properties.

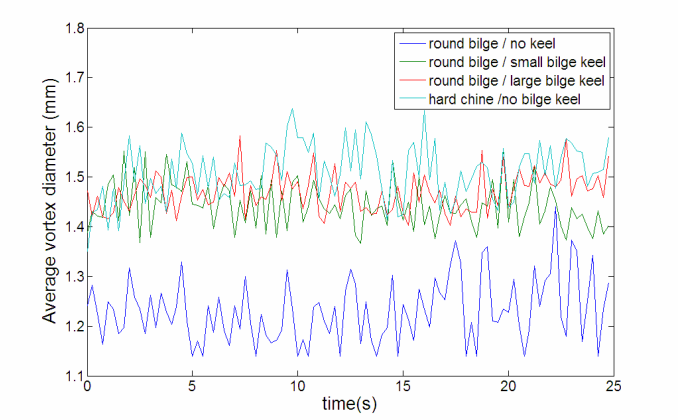

Figure 6. Temporal evolution of the average vortex diameter

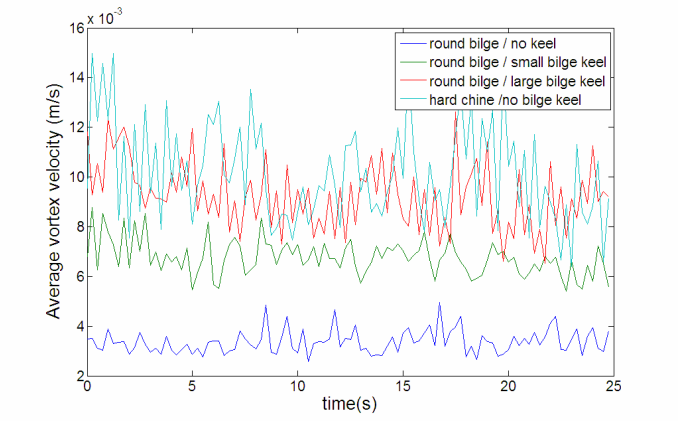

Figure 7. Temporal evolution of the average vortex velocity

ISSN 2176-5480

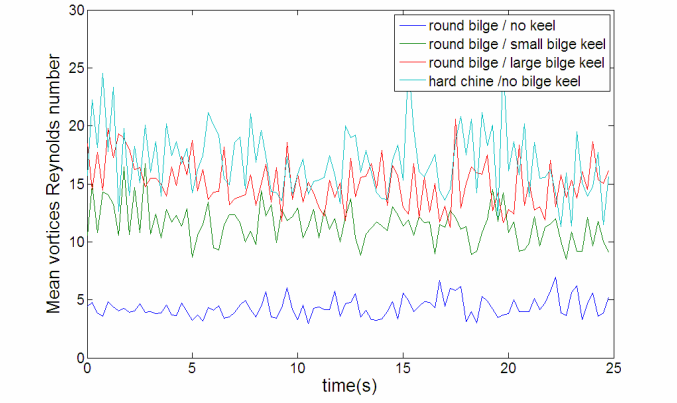

Figure 8. Temporal evolution of the average Reynolds number

Figure 8 is specially informative. As we can observe, the flow field induced by every one of the cylindrical rolling bodies is clearly turbulent, since the least average vortex Reynolds number found in this graphic is higher than ≈1 (Davidson, 2007). Furthermore, the temporal evolution graphs of this property indicates that the four tested cylindrical bodies exhibit a clear ranking of energy dissipation, starting from the less effective (round bilge without bilge keel) and progressively increasing as we aggregate bilge keels to the hull or adopt a hard-chine hullform. Those achievements are in full agreement with the literature (Souza Jr. et al., 1998; Ferrari Jr. and Ferreira, 2002; Fernandes and Oliveira, 2009) concerning the significant effect of bilge keels in diminishing the damping coefficient of a floating body undergoing rolling motion.

At a grabbing image rate of 4 Hz – only two times the forced rolling frequency (2 Hz) of the models, reliable modal information of the signals from Figs. 6-8 could not be obtained from the power spectra, except a confirmation that vortices with larger diameters, velocities and Reynolds numbers are emitted at the forced frequency, as expected (see Fig. 9, where larger peaks of Reynolds numbers are observed at the 2 Hz frequency).

Future experiments must overcome this difficult by adopting an image frame rate at least 4 times the forced rolling frequency, in order to capture information from the first three harmonics of the signals.

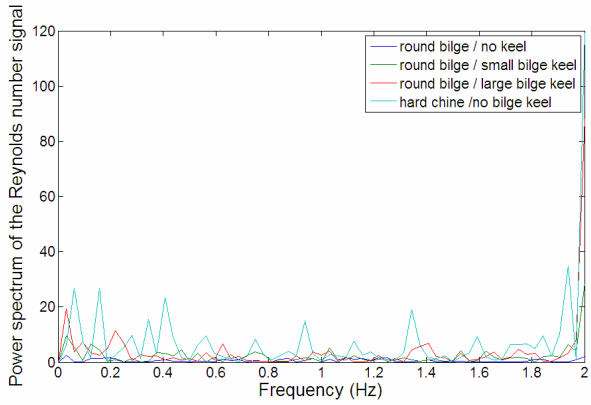

Figure 9. Power spectrum of the Reynolds number signal

6. CONCLUSIONS

The analysis of PIV images representative of flow fields generated by harmonically forced rolling motions of four different cylindrical bodies (three 'round bilge', either with or without a bilge keel, one 'hard chine') permitted to identify the vorticity regions of the flows, perform local vortex measures concerning diameter (*D*), velocity (*V*) and Reynolds (*Re*) number and, as a consequence, estimate average metrics $\overline{D}(t), \overline{V}(t), \overline{\mathrm{Re}}(t)$ whose temporal evolution may give rise to a criterium to compare the hydrodynamical performance of the hulls concerning rolling motion.

As expected, an increasing ranking of *rms* values for $\overline{D}(t)$, $\overline{V}(t)$, and $\overline{\mathrm{Re}}(t)$ could be observed respectively for the ´round bilge' , 'round bilge with small bilge keel', 'round bilge with large bilge keel' and 'hard chine no bilge keel' hulls. However, a deeper analysis of the spectral characteristics of those signals could not be performed due to the small image frame rate used during the tests, a drawback that will be eliminated in future investigations.

7. ACKNOWLEDGEMENTS

This work was supported by FINEP – Financiadora de Estudos e Projetos, as part of the project "Desenvolvimento tecnológico colaborativo de ferramenta de projeto para avaliação do desempenho hidrodinâmico de embarcações submersas" (CT-Aquaviário Convênio 0577/10). Third author also gratefully acknowledges CNPq – Conselho Nacional de Desenvolvimento Científico e Tecnológico, for finantial support.

8. REFERENCES

Adrian, R.J., Christensen, K.T., Liu, Z.C., Analysis and interpretation of instantaneous turbulent velocity fields. Experiments in Fluids, 29, 2000, p. 275-290.

Baur, T., Koengeter, J., High-speed PIV and the post-processing of time-series results. Proceedings of the EuroMech 411 – Application of PIV to turbulence measurements, developments of 3D stereoscopic and holographic techniques, 2000, 5p.

Chakraborty, P., Balachandar, S., Adrian, R., On the relationships between local vortex identification schemes. Journal of Fluid Mechanics, Vol.535, 2005, p. 189-214.

Davidson, P.A., Turbulence: An Introduction for Scientists and Engineers. Oxford University Press, 2007.

Fernandes, A.C., Oliveira, A.C., The roll damping assessment via decay model testing (new ideas about an old subject). Journal of Marine Science and Application, vol.8, 2009, pp. 144-150.

Ferrari Jr., J.A.,. Ferreira, M.D.A., Assessment of the effectiveness of the bilge keel as an anti-rolling device in VLCC-sized FPSOs. Proceedings of the 12th International Offshore and Polar Engineering Conference, Kitakyushu, Japan, May, 26-31, 2002, pp. 107-113.

Finn, L.I., Boghosian, B.M., Kottke, C.N., Vortex core identification in viscous hydrodynamics. Philosophical Transactions of Royal Societiy, Series A, Mathematical, Physical and Engineering Series, 15, Vol. 363, n.1833, Aug. 2005, p. 1937-1948.

Haralick, R.M., Shapiro, M., Computer and Robot Vision. Addison Wesley, 1991.

Horn, B.K.P., Robot Vision, 2nd ed. The MIT Press, 1986.

Jiang., M., Machiraju, R., Thompson, D., Detection and visualization of vortices. In The Visualization Handbook. Hanse, CD., Johnson, C.R., editors. Academic Press, 2004.

Kolár, V., Vortex identification: new requirements and limitations. International Journal of Heat and Fluid Flow, 28, 2007, p. 638-652.

Niblack, W., An Introduction to Digital Image Processing. Prentice-Hall, 1986.

Nogueira, J., Lecuona, A., Rodríguez, P.A., Data validation, false vectors correction and derived magnitudes calculation on PIV data. Measurement, Science and Technology, 8, 1997, p. 1493-1501.

Otsu, N., A threshold selection method from gray-level histograms. IEEE Transactions on Systems, Man and Cybernetics, v.SMC-9, nº 1, Jan. 1979, p.62-66.

Rao, A.R., Jain, R.C., Computerized flow field analysis: oriented texture fields. IEEE Transactions on Pattern Analysis and Machine Intelligence, Vol.14, n. 7, July 1992, p. 693-709.

Serra, J., Image Analysis and Mathematical Morphology, v.1. 3rd ed. Academic Press, 1989.

Souza Jr., J.R., Fernandes, A.C., Masetti, I.Q., da Silva, S., Kroff, S.A.B., Nonlinear rolling of an FPSO with larger than usual bilge keels. Proceedings of the 17th International Conference on Offshore Mechanics and Arctic Engineering (OMAE), Lisbon, 1998, pp. 100-112.

Yang, Q., Wang, J., Liu, Z., Bao, F., Application of median filtering on PIV images analysis. Proceedings of The International Conference on Computer Science and System Service – CSSS, 2011, p. 2108-2011.

9. RESPONSIBILITY NOTICE

The authors are the only responsible for the printed material included in this paper.